



## Copyright Notice

This paper was published in *Optics Letters* and is made available as an electronic reprint with the permission of OSA. The paper can be found at the following URL on the OSA website: <http://dx.doi.org/10.1364/OL.37.000100>. Systematic or multiple reproduction or distribution to multiple locations via electronic or other means is prohibited and is subject to penalties under law.

*(Article begins on next page)*

# Diffraction from carbon nanofiber arrays

R. Rehammar,<sup>1,\*</sup> Y. Francescato,<sup>2</sup> A. I. Fernández-Domínguez,<sup>2</sup> S. A. Maier,<sup>2</sup>  
J. M. Kinaret,<sup>1</sup> and E. E. B. Campbell<sup>3,4</sup>

<sup>1</sup>Department of Applied Physics, Chalmers University of Technology, SE-41296 Gothenburg, Sweden

<sup>2</sup>Department of Physics, Imperial College London, London SW72AZ, United Kingdom

<sup>3</sup>EaStCHEM, School of Chemistry, Edinburgh University, Edinburgh EH9 3JJ, Scotland

<sup>4</sup>Division of Quantum Phases and Devices, Department of Physics, Konkuk University, Seoul 143-701, Korea

\*Corresponding author: robert.rehammar@chalmers.se

Received September 14, 2011; revised October 25, 2011; accepted November 15, 2011;

posted November 17, 2011 (Doc. ID 154340); published December 24, 2011

A square planar photonic crystal composed of carbon nanofibers was fabricated using e-beam lithography and chemical vapor deposition. The diffraction properties of the system were characterized experimentally and compared with theory and numerical simulations. The intensities of the  $(-1, 0)$  and  $(-1, -1)$  diffraction beams were measured as functions of the angles of incidence for both  $s$  and  $p$ -polarization. The obtained radiation patterns can be explained using a simple ray interference model, but finite-difference time-domain (FDTD) calculations are necessary to reproduce the observed dependence of the scattered radiation intensity on incident laser polarization. We explain this in terms of the aspect ratio of the nanofibers and the excitation of surface plasmon polaritons at the substrate interface. © 2011 Optical Society of America

OCIS codes: 050.6624, 050.5298, 050.1960, 050.1970.

Photonic crystals (PCs) have emerged as exciting optical systems with promising properties, such as the ability to have ultra slow light propagation [1], negative refraction [2], and extreme light confinement [3]. Recently, there has been an increasing interest in developing antennas operating in the optical regime [4–7], which requires the fabrication of structures with controlled dimensions on the order of the wavelength of visible light. One convenient way to achieve two-dimensional PC slabs operating in the optical range is to grow arrays of nanowires or carbon nanofibers (CNF) using plasma enhanced chemical vapor deposition (PECVD). The pattern of the structures can be controlled by lithographic deposition of nanoscale metal particles that seed the PECVD growth [8]. An additional advantage of using conducting CNFs is that they can potentially be electrically actuated, providing a convenient and practical means of tuning the optical properties of the PCs. In order to achieve this, it is necessary to grow the CNFs on conducting substrates and first understand the optical properties of the static arrays that can be produced.

CNF arrays grown on Si have been shown earlier to work as diffraction gratings when irradiated with white light [9,10], and light transmission through nanowire-based PCs has been studied theoretically [11]. We have recently shown that variable-angle spectroscopic ellipsometry can be used to determine the band structure of CNF PCs on a metallic substrate [12]. In this Letter, the fundamental diffraction properties of CNF-based PCs are studied in detail. We report experimental and theoretical investigations of light diffraction from a square CNF array. We show that a simple theoretical model of the form factor of the lattice can be used to describe the angular dependent intensity variations observed in the diffracted beams. We also observe clear polarization-dependent intensity variations that cannot be explained with our ray interference model. The origin of these effects is revealed by finite-difference time-domain (FDTD) calculations that highlight the influence of the detailed structure of

the CNFs and the excitation of surface plasmons in the metal substrate.

A sample consisting of a CNF square array with lattice constant  $a = 500$  nm is shown Fig. 1(a). CNFs are grown to a height of approximately  $1.4 \mu\text{m}$  with a diameter of 65 nm. A more detailed description of the fabrication process can be found elsewhere [13,12]. When light interacts with an ordered array of scatterers, an integer multiple of a reciprocal lattice vector can be transferred by the lattice to the incident wave [14]. We denote the incoming wave vector  $\mathbf{k}$  and the diffracted wave vector  $\mathbf{k}'$ . For incoming light with in-plane wave vector  $\mathbf{k}_{\parallel} = (k_x, k_y)$ , the

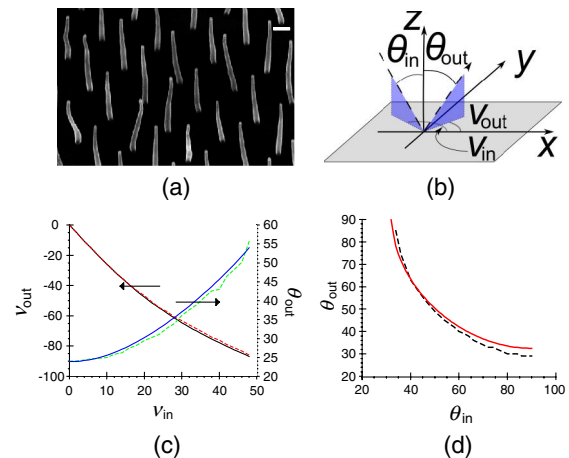


Fig. 1. (Color online) (a) SEM micrograph of a CNF lattice. Scale bar is 200 nm. (b) Definitions of the measured angles. The gray plane represents the sample surface, and the dashed line represents the incoming and reflected light. The inclination angle,  $\Theta_{\text{in}}$ , and exiting angle,  $\Theta_{\text{out}}$ , are measured from the sample normal. Azimuthal angles,  $\nu_{\text{in}}$  and  $\nu_{\text{out}}$ , for the incident and diffracted light, respectively, are measured from the  $x$ -axis. (c) Theoretical (solid) and experimental (dashed) relation between the diffracted and incident azimuthal angles for the  $(m, n) = (-1, 0)$  order and  $\Theta_{\text{in}} = 43^\circ$ . (d) Diffracted versus incident inclination angles obtained from theory (solid) and experiment (dashed) for  $(m, n) = (-1, -1)$  and  $\nu_{\text{in}} = 45^\circ$ .

diffracted in-plane wave vectors are given by  $\mathbf{k}'_{\parallel} = (k_x + mG, k_y + nG)$ , where  $m$  and  $n$  are integers and  $G = 2\pi/a$ . Energy conservation gives that  $|\mathbf{k}'|^2 = |\mathbf{k}|^2$ . This yields the following constraint on  $k'_z$ :

$$k'_z{}^2 = k_z^2 - G^2(m^2 + n^2) - 2G(mk_x + nk_y). \quad (1)$$

A green ( $\lambda = 543.5$  nm) HeNe laser is used to study the interaction of light with the CNF array. In the measurement process, one of the incident angles,  $\Theta_{\text{in}}$  or  $\nu_{\text{in}}$ , is fixed while varying the other, and the exiting angles,  $\Theta_{\text{out}}$  and  $\nu_{\text{out}}$ , are recorded accordingly (see Fig. 1(b) for angle definition). The lower panels of Fig. 1 show the relation between diffracted and incident angles in two different configurations (note that  $\nu_{\text{in}} = 45^\circ \Rightarrow \nu_{\text{out}} \equiv 45^\circ$  in panel (d)). The excellent agreement between the theoretical prediction from Eq. (1) (solid line) and measurements (dashed line) in both cases indicates the regular geometric design of the samples.

Only those diffracted waves having  $k'_z$  real are scattered out of the structure and reirradiated into free space. According to Eq. (1), for the experimental conditions ( $a = 500$  nm,  $\lambda = 543.5$  nm) only  $(m, n) = (-1, 0) \equiv (0, -1)$  and  $(-1, -1)$  fulfill  $k'_z{}^2 > 0$ . In agreement with this, only reflected beams along the directions associated with these diffraction orders are observed in our experiment. However, while Eq. (1) predicts correctly the measured diffraction directions, it does not give us any information about the actual intensity profile associated with each reflected beam. In our experiment, we fix the incident azimuthal angle to  $0^\circ$  and  $45^\circ$ , which allows us to probe the reflected radiation profile for  $(m, n) = (-1, 0)$  and  $(-1, -1)$ , respectively. Thus, by varying the incident inclination angle, light intensity can be recorded for different  $\Theta_{\text{out}}$ .

The red circles in Fig. 2 show the measured diffraction intensity (in log scale) as a function of  $\Theta_{\text{in}}$  for  $(m, n) = (-1, 0)$  (top) and  $(-1, -1)$  (bottom), and for  $p$  (left) and  $s$  (right) incident polarizations. These plots demonstrate that the radiation intensity depends strongly on the incident angle, presenting a main lobe whose direction changes with diffraction order, and much weaker lateral side-lobes, highlighted in Fig. 2 by the use of a log scale. Light diffracted by the CNF lattice accumulates a phase which depends on where the interaction occurs on the CNF extension. Equation (1) does not impose any sign restriction on  $k'_z$ , yielding diffraction in both positive and negative  $z$ -directions. Thus, the incident light can be directly reflected by the CNFs or can propagate through it, getting reflected at the substrate. The interference of these two diffraction channels gives an outgoing electric field proportional to

$$E \sim \int_0^H dz (e^{i\Delta l_1} + e^{i\Delta l_2}), \quad (2)$$

where the integration is performed along the length of the CNF,  $H = 1.4$   $\mu\text{m}$ , and  $\Delta l_1$  and  $\Delta l_2$  are the two different optical path lengths for light propagating in the positive and negative  $z$ -directions. Note that Eq. (2) is closely related to what is known in diffraction theory as the form factor [14]. In [15], similar scattering proper-

ties of individual CNFs have been analyzed in the framework of antenna theory.

The intensity profile resulting from Equation (2) is sensitive to  $h = H/\lambda$ , which determines the number of side-lobes and the power distribution within the radiation pattern. Solid black lines in the four plots shown in Fig. 2 give the electric field intensity obtained from the ray interference model. The comparison between theory and measurements is very good, and the excellent agreement in the main lobe direction is remarkable. This demonstrates that our model describes the fundamental physics behind the diffraction properties of the experimental CNF samples.

Although our interference model reproduces the main features of the measured radiation profiles, it does not take into account the effect of the incident polarization. The experimental data in Fig. 2 show an intensity decrease (of the order of 60–70% at the main lobe maximum) when the sample is illuminated with  $p$ -polarized light compared to the intensity with  $s$ -polarized excitation. In order to investigate the origin of this polarization effect, we performed numerical simulations using Lumerical, a commercial software implementing the FDTD algorithm. The diffraction patterns are plotted as triangles in Fig. 2. The polarization-dependent intensity difference is reproduced by the FDTD calculations, showing a decrease of 30–70% for  $p$ -polarized light. The FDTD results are found to be critically dependent on the aspect ratio of the CNF (where we use the values obtained from scanning electron microscope (SEM) studies of the experimental substrates) and also require the inclusion of the Ni catalyst particle at the tip of the CNF to get satisfactory agreement with experiment. Note that theoretical

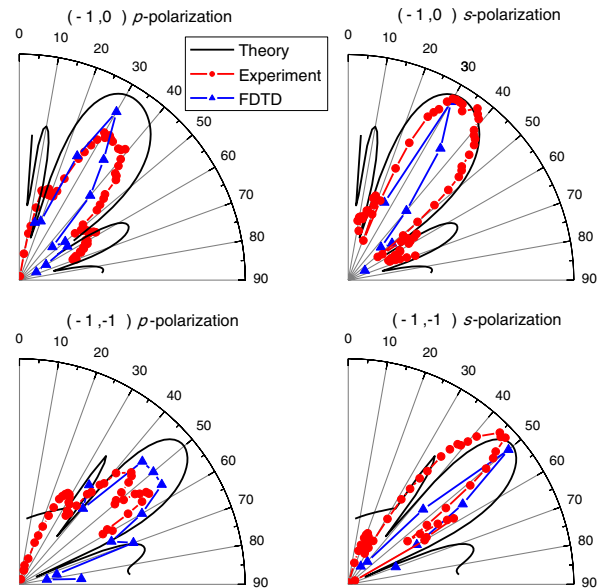


Fig. 2. (Color online) Polar plots rendering the normalized electric field intensity in log scale as a function of  $\Theta_{\text{in}}$  within the plane of incidence in four different cases. Upper and lower panels correspond to the  $(-1, 0)$  and  $(-1, -1)$  diffracted beams, respectively, and left (right) panels show radiation patterns for  $p$  ( $s$ ) incident polarization. In each panel, three different data sets are shown: measurements (red circles), numerical simulations (blue triangles), and the theoretical prediction from the ray interference model (black solid line).

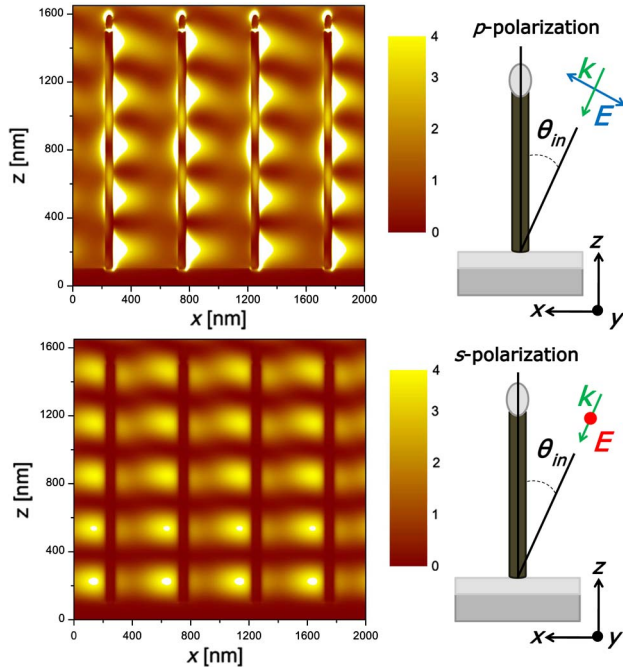


Fig. 3. (Color online) Near field maps within the plane of incidence ( $\Theta_{in} = 30^\circ$ ) corresponding to the  $(-1, 0)$  diffraction order for incident  $p$  (upper panel) and  $s$  (lower panel) polarization (see right schematic pictures). Both panels consist of four PC unit cells and show the electric field intensity in linear scale.

and simulated results in Fig. 2 are normalized to the experimental data for incident  $s$ -polarization.

In order to elucidate the origin of polarization effects, in Fig. 3, the near field intensity is plotted for the  $(-1, 0)$  case. The upper (lower) panel shows the electric field intensity (in linear scale) within the incident plane comprising four PC unit cells under  $p$  ( $s$ ) polarization. Note that the field intensity at the CNFs is much higher for  $p$ -polarization. This is due to the hybridization of surface plasmon polaritons [16], which are mainly  $p$ -polarized excitations, at the Ti-TiN substrate with the surface modes of the CNF PC. The confined character of these  $p$ -polarized electromagnetic modes makes them very sensitive to metal absorption, which explains the lower reflection intensity observed in experiments and FDTD simulations for both diffraction orders under  $p$ -polarized illumination.

To conclude, we have investigated diffractive properties of CNF-based PCs. We have shown that standard diffraction theory can be used to describe the main reflection angles but cannot explain the polarization-

dependent diffracted intensities. The origin of the polarization effects was revealed from the form factor of the CNF array and the role of surface plasmons at the PC-substrate interface. The kind of nano-optical systems investigated in this work show promise as tunable optical antennas where the radiation direction and intensity of visible light can be controlled on the nano scale.

This work was sponsored in part by the Engineering and Physical Sciences Research Council (EPSRC). R. Rehammar, J. M. Kinaret and E. E. B. Campbell acknowledge funding from the Swedish Foundation for Strategic Research (SSF).

## References

1. Y. A. Vlasov, M. O'Boyle, H. F. Hamann, and S. J. McNab, *Nature* **438**, 65 (2005).
2. E. Cubukcu, K. Aydin, E. Ozbay, S. Foteinopoulou, and C. M. Soukoulis, *Nature* **423**, 604 (2003).
3. T. Yoshie, J. Vuckovic, A. Scherer, H. Chen, and D. Deppe, *Appl. Phys. Lett.* **79**, 4289 (2001).
4. P. Muhlschlegel, H. J. Eisler, O. J. F. Martin, B. Hecht, and D. W. Pohl, *Science* **308**, 1607 (2005).
5. Y. Wang, K. Kempa, B. Kimball, J. B. Carlson, G. Benham, W. Z. Li, T. Kempa, J. Rybczynski, A. Herczynski, and Z. F. Ren, *Appl. Phys. Lett.* **85**, 2607 (2004).
6. P. Bharadwaj, B. Deutsch, and L. Novotny, *Adv. Opt. Photon.* **1**, 438 (2009).
7. V. Giannini, A. I. Fernández-Domínguez, S. C. Heck, and S. A. Maier, *Chem. Rev.* **111**, 3888 (2011).
8. M. S. Kabir, R. Morjan, O. Nerushev, P. Lundgren, S. Bengtsson, P. Enoksson, and E. Campbell, *Nanotechnology* **17**, 790 (2006).
9. K. Kempa, B. Kimball, J. Rybczynski, Z. Huang, P. Wu, D. Steeves, M. Sennett, M. Giersig, D. Rao, D. Carnahan, D. Wang, J. Lao, W. Li, and Z. Ren, *Nano Lett.* **3**, 13 (2003).
10. J. Rybczynski, K. Kempa, Y. Wang, Z. F. Ren, J. B. Carlson, B. R. Kimball, and G. Benham, *Appl. Phys. Lett.* **88**, 203122 (2006).
11. R. Rehammar and J. M. Kinaret, *Opt. Express* **16**, 21682 (2008).
12. R. Rehammar, R. Magnusson, A. I. Fernández-Domínguez, H. Arwin, J. M. Kinaret, S. A. Maier, and E. E. B. Campbell, *Nanotechnology* **21**, 465203 (2010).
13. R. Rehammar, R. Magnusson, A. Lassesson, H. Arwin, J. Kinaret, and E. Campbell, *MRS Proc.* **1283** (2011).
14. C. Kittel, *Introduction to Solid State Physics*, 7th ed. (John Wiley and Sons, 1996).
15. K. Kempa, J. Rybczynski, Z. Huang, K. Gregorczyk, A. Vidan, B. Kimball, J. Carlson, G. Benham, Y. Wang, A. Herczynski, and Z. Ren, *Adv. Mater.* **19**, 421 (2007).
16. S. A. Maier, *Plasmonics: Fundamentals And Applications* (Springer Verlag, 2007).